



## AMORPHOUS PHASE FORMING ABILITY IN (W–C)-BASED SPUTTERED FILMS

B. TRINDADE<sup>1</sup>, M. T. VIEIRA<sup>1</sup> and E. BAUER-GROSSE<sup>2</sup>

<sup>1</sup>ICEMS, Departamento de Engenharia Mecânica, Faculdade de Ciências e Tecnologia, Universidade de Coimbra, 3030 Coimbra, Portugal and <sup>2</sup>Laboratoire de Science et Génie des Surfaces de l'Ecole Nationale Supérieure des Mines de Nancy, 54042 Nancy, France

(Received 13 March 1997; accepted 5 September 1997)

**Abstract**—The effect of adding transition metals, Me, to the structure of (W–C)-based films obtained by sputtering has been studied by the means of electron probe microanalysis (EPMA), secondary ion mass spectrometry (SIMS), low angle X-ray diffraction (XRD), hot stage transmission electron microscopy (TEM), Mössbauer spectroscopy, extended X-ray absorption fine structure (EXAFS), magnetic measurements and differential thermal analysis (DTA). The results obtained for the films in the as-deposited conditions show two types of structures with different degrees of structural order. Films with Ti, Cr or Au are crystalline with a metastable structure of  $\beta$ -(W<sub>1-x</sub>Me<sub>x</sub>)C<sub>1-x</sub> with 1-x extending from near unity down to about 0.6. In opposition to these, films with Me = Group VIIIA transition metal, show crystalline → amorphous state transitions for Me percentages in the range 5–10 at.%. The structure of these films consists of small  $\beta$ -MC<sub>1-x</sub> crystallites with a size of a few unity cells, surrounded by a disordered phase rich in element Me. Concerning the results obtained at increasing temperatures, the chemical and structural behaviour of the W–Me–C films depend on the affinity of carbon for the element Me. Strong or moderate carbide-forming elements (Ti or Cr) improve the stability of the crystalline phase at high temperatures; the films formed by W, C and a weak or non carbide-forming metal (Fe, Co, Ni, Pd or Au) change structurally in the temperature range studied. © 1998 Acta Metallurgica Inc.

### 1. INTRODUCTION

Transition metal carbides find wide technological applications as wear resistant coatings on a variety of surfaces such as cemented tools and steel. Much effort has been devoted over the last few years to studying (W–C)-based films obtained by sputtering from sintered materials [1–8]. Previous work concerning the synthesis of W–(Fe,Co)–C [6] and W–Ni–C [7] films by sputtering showed that the microstructure of these materials is affected by the level of addition of element Me. When obtained from a sintered stoichiometric WC target, the structure of the sputtered films is formed by small grains of  $\beta$ -WC<sub>1-x</sub>, with  $x \approx 0.15$ ; the co-deposition of WC with iron, cobalt or nickel induces amorphization of the structure for concentrations of Me in the range 5–10 at.%. The atomic arrangement of these amorphous alloys is not completely random, but maintains a certain degree of structural order (less than 20 Å) [6–8]. The tendency to produce amorphous W–Me–C materials by Group VIIIA elements was explained by both size difference between the constituent metals of the films (W and Fe or Co or Ni) and weakening of the carbon–metal bonds by the presence of a metallic element with a lower affinity for carbon than tungsten. Guided by these results, and in order to confirm these concepts, it is important to study the influence of other transition metals in both the as-deposited and annealed structure of

sputtered (W–C)-based materials. For this purpose, transition metals from Groups IVA–IB (Ti, Cr, Pd and Au) were used as additions to W–C films. These metals were chosen keeping in mind their atomic radii and affinity for carbon: the atomic size differences between them and tungsten are less than 10%; however, they have different carbon affinities (contrarily to palladium and gold, titanium and chromium are carbide-formers).

This work reports the influence of different Me solute metallic atoms (Me = Ti, Cr, Fe, Co, Ni, Pd and Au) on the as-deposited structure of (W–C)-based systems and their annealing behaviour. The films were synthesised from (W–C) + Me targets by non-reactive sputtering under the same conditions described in [6]. Chemical and structural analysis of the as-deposited films were performed by means of electron probe microanalysis (EPMA), secondary ion mass spectrometry (SIMS), low angle X-ray diffraction (XRD) and transmission electron microscopy (TEM). In order to determine the atomic arrangement of the crystalline and amorphous (W–C)-based films, Mössbauer spectroscopy, extended X-ray absorption fine structure (EXAFS) and magnetic measurements were carried out on the as-deposited W–Fe–C films. The study of the influence of different carbide formers on the annealing behaviour of (W–C)-based systems was performed on W–Me–C films with Me = Ti, Cr, Fe, Co, Ni and Au. Films on substrates which were annealed at

Table 1. Chemical composition (at.%) of synthesised W–Me–C films

Group IVA	Group VIA	Group VIIIA				Group IB
Me = Ti	Me = Cr	Me = Fe	Me = Co	Me = Ni	Me = Pd	Me = Au
W <sub>59</sub> Ti <sub>3</sub> C <sub>38</sub>	W <sub>56</sub> Cr <sub>6</sub> C <sub>38</sub>	W <sub>52</sub> Fe <sub>4</sub> C <sub>44</sub>	W <sub>53</sub> Co <sub>4</sub> C <sub>43</sub>	W <sub>56</sub> Ni <sub>4</sub> C <sub>40</sub>	W <sub>53</sub> Pd <sub>4</sub> C <sub>43</sub>	W <sub>52</sub> Au <sub>6</sub> C <sub>42</sub>
W <sub>56</sub> Ti <sub>8</sub> C <sub>36</sub>	W <sub>50</sub> Cr <sub>11</sub> C <sub>39</sub>	W <sub>52</sub> Fe <sub>6</sub> C <sub>42</sub>	W <sub>52</sub> Co <sub>6</sub> C <sub>42</sub>	W <sub>53</sub> Ni <sub>6</sub> C <sub>41</sub>	W <sub>50</sub> Pd <sub>7</sub> C <sub>43</sub>	W <sub>49</sub> Au <sub>11</sub> C <sub>40</sub>
W <sub>45</sub> Ti <sub>15</sub> C <sub>40</sub>	W <sub>48</sub> Cr <sub>14</sub> C <sub>38</sub>	W <sub>46</sub> Fe <sub>13</sub> C <sub>41</sub>	W <sub>48</sub> Co <sub>13</sub> C <sub>39</sub>	W <sub>50</sub> Ni <sub>10</sub> C <sub>40</sub>	W <sub>46</sub> Pd <sub>12</sub> C <sub>42</sub>	W <sub>47</sub> Au <sub>15</sub> C <sub>38</sub>
W <sub>40</sub> Ti <sub>26</sub> C <sub>34</sub>	W <sub>46</sub> Cr <sub>17</sub> C <sub>37</sub>	W <sub>42</sub> Fe <sub>20</sub> C <sub>38</sub>	W <sub>44</sub> Co <sub>18</sub> C <sub>38</sub>	W <sub>47</sub> Ni <sub>15</sub> C <sub>38</sub>	W <sub>43</sub> Pd <sub>16</sub> C <sub>41</sub>	W <sub>43</sub> Au <sub>23</sub> C <sub>34</sub>
W <sub>36</sub> Ti <sub>34</sub> C <sub>30</sub>	W <sub>45</sub> Cr <sub>21</sub> C <sub>34</sub>	W <sub>36</sub> Fe <sub>31</sub> C <sub>33</sub>	W <sub>38</sub> Co <sub>22</sub> C <sub>40</sub>	W <sub>39</sub> Ni <sub>23</sub> C <sub>38</sub>	W <sub>33</sub> Pd <sub>33</sub> C <sub>32</sub>	W <sub>38</sub> Au <sub>32</sub> C <sub>30</sub>

650, 700 and 750°C were analysed after each thermal cycle by EPMA and XRD. Concomitantly, DTA measurements were carried out on films detached from the substrates within the temperature range of 20–1000°C. The structure of these 1000°C annealed films was subsequently determined by XRD.

## 2. EXPERIMENTAL DETAILS

The W–Me–C films were non-reactively r.f. sputtered onto steel and glass substrates from WC + Me (Me = Ti, Cr, Fe, Co, Ni, Pd, Au) targets. Films on steel substrates were examined in the as-deposited state and after 1 h furnace annealing under vacuum ( $P = 10^{-5}$  Pa) at temperatures of 650, 700 and 750°C. The chemical composition of the films was determined before and after each heat treatment by EPMA. The composition–depth profiles of the films were determined by SIMS using Cs<sup>+</sup> primary ions. XRD results were obtained with Co K $\alpha$ 1 radiation at an incident angle of 4°. TEM analysis of films detached from the glass substrates was performed in a 200 keV microscope. The films were thinned on both sides to electron transparency by ion-milling. Mössbauer spectroscopy, EXAFS and magnetic measurements were applied to the W–Fe–C as-deposited films. The <sup>57</sup>Fe Mössbauer measurements were performed in transmission geometry by means of a spectrometer with a constant acceleration velocity. Calibration was done with a metallic iron foil. EXAFS experiments were performed at the “Laboratoire pour l’Utilisation du

Rayonnement Electromagnétique (LURE)” on the surface monochromator installed on the DCI storage ring. Magnetic measurements were carried out in a conventional Gouy balance. DTA analysis was performed within the temperature range 20–1000°C at a continuous heating rate of 0.25°C/s.

## 3. RESULTS

### 3.1. As-deposited state

The chemical composition of the as-deposited films is summarized in Table 1. The films are carbon-deficient with W/C atomic ratios higher than unity (Fig. 1). In the majority of the W–Me–C systems, the carbon deficit in the films decreases with the increase of the Me percentage. The W–Au–C system is the only exception to this: the higher the gold content, the higher is the carbon deficit.

The SIMS composition–depth profiles of the synthesised W–Me–C films do not change from the surfaces to the film/substrate interfaces (Fig. 2). These are well defined, suggesting the non-existence of a chemical reaction between the films and the steel substrate.

The structural results of the as-deposited W–Me–C films are presented in Figs 3–6. Figure 3 shows a compilation of both XRD and TEM results, where it can be seen that the structure of the W–Me–C films depends on the type and concentration of the metal Me. All the W–Me–C films with Me = Ti,

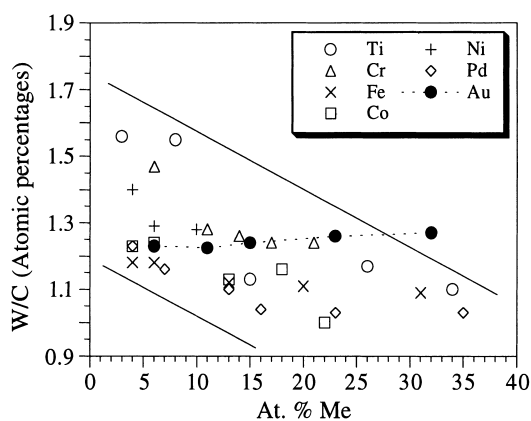


Fig. 1. Carbon-deficit of the various W–Me–C systems as a function of the Me content in the films.

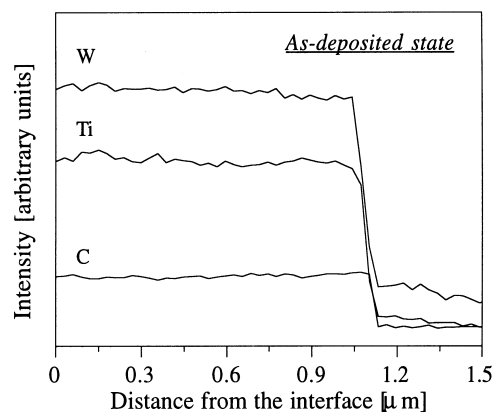
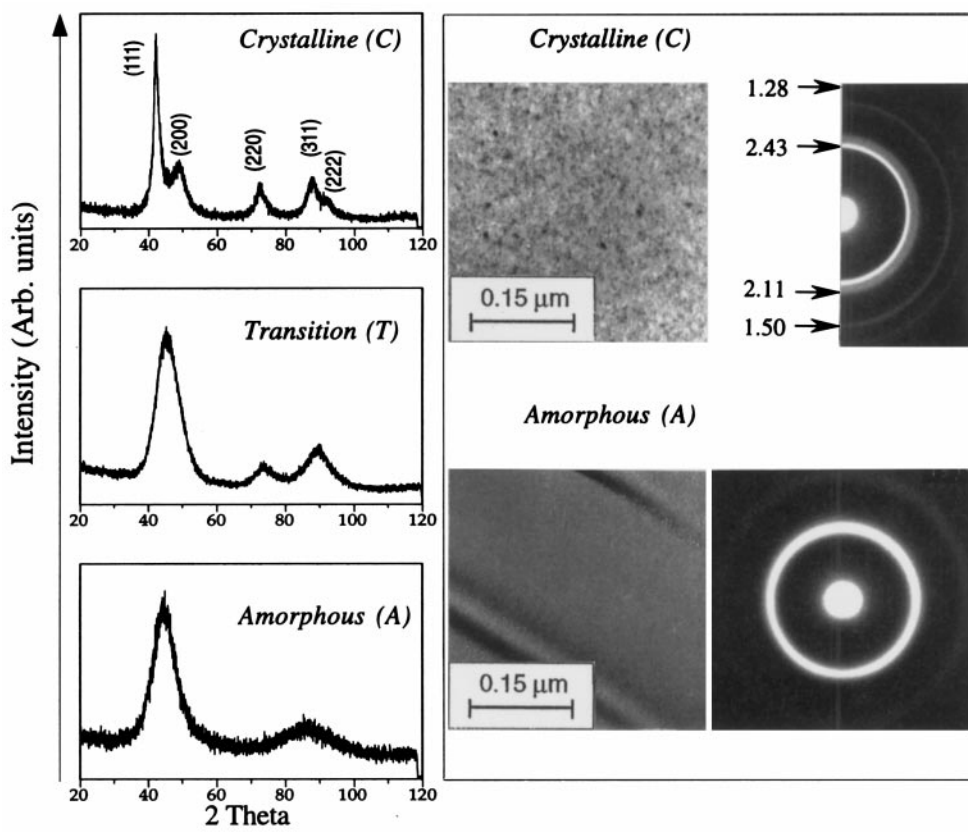


Fig. 2. Typical SIMS sputter depth profiles for the as-deposited W–Me–C films deposited onto high-speed steel substrates. These profiles were taken from a W<sub>56</sub>Ti<sub>8</sub>C<sub>36</sub> film.



	IVA	VIA	VIII A				IB
	Ti	Cr	Fe	Co	Ni	Pd	Au
0	C	C	C	C	C	C	C
10	C	C	T	T	T	T	C
20	C	C	A	A	A	A	C
30	C	C	A	A	A	A	C
40	C	C	A	A	A	A	C

C = Crystalline    T = Transition    A = Amorphous

Fig. 3. Compilation of both XRD and TEM structural results of W-Me-C films.

Cr or Au are formed by a fine-grained crystalline f.c.c. structure of  $\beta$ - $MC_{1-x}$  ( $M = W, Me$ ), characterized by five relatively broad X-ray diffraction peaks and large electron diffraction (ED) rings. However, films with  $Me = Metal\ of\ Group\ VIII\ A$  become progressively amorphous with increasing Me content; the crystalline  $\rightarrow$  amorphous structural transition occurs for Me concentrations in the range 5–10 at.%. Similar to W-Me-C ( $Me = Ti, Cr, Au$ ) films, the crystalline W-(Fe,Co,Ni,Pd)-C films are formed by fine grained NaCl-type structure. The amorphous films are characterized by

two very broad X-ray peaks (a stronger broad peak and a weaker sub-peak) and low contrast TEM images associated with diffuse and large ED rings.

Figure 4 shows the room temperature Mössbauer spectra obtained for two W-Fe-C films as typical examples of the different structural states (crystalline and amorphous). The spectra were fitted with a certain number of Lorentzian curves on the basis of both XRD and TEM results. The crystalline films were fitted with two symmetric doublets, corresponding to different structural configurations around the iron atom (see Ref. [5]); the amorphous

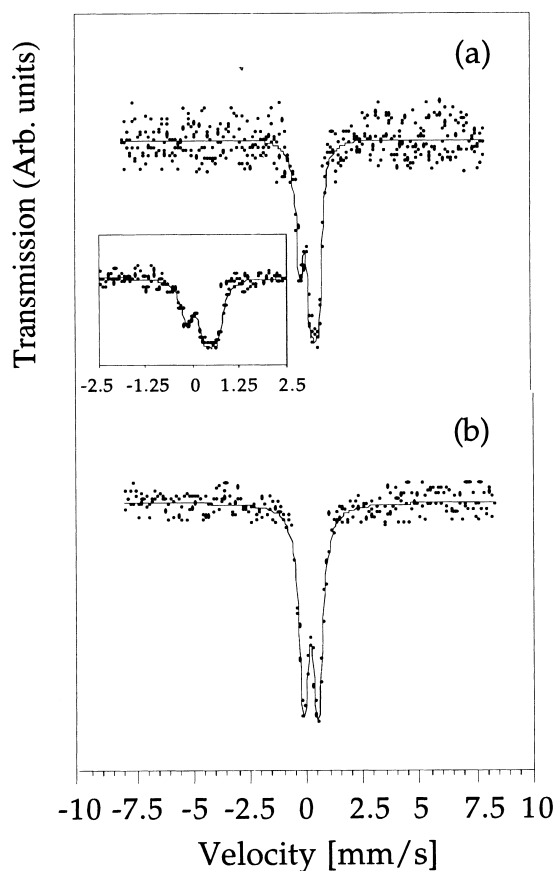


Fig. 4. Mössbauer spectra taken from (a) film  $W_{53}Fe_4C_{44}$ , (b) film  $W_{42}Fe_{20}C_{38}$ .

films were fitted with two independent curves. The hyperfine parameters (isomer shift and quadrupole splitting) obtained for the W-Fe-C films are given in Fig. 5. The isomer shift (I.S.) decreases with the increase of the iron content in the films. The quadrupole splitting (Q.S.) of the crystalline films is higher than that of the amorphous films and it decreases in both structural domains.

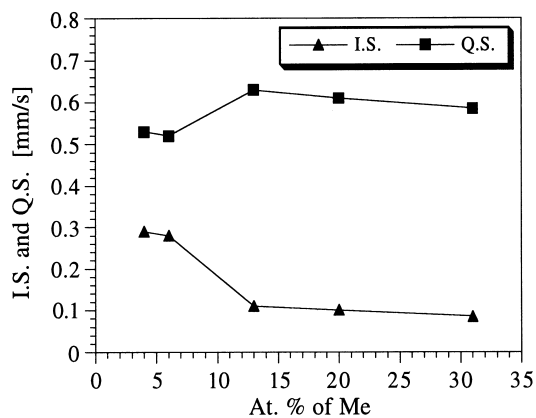


Fig. 5. Mössbauer hyperfine parameters obtained for the W-Fe-C films.

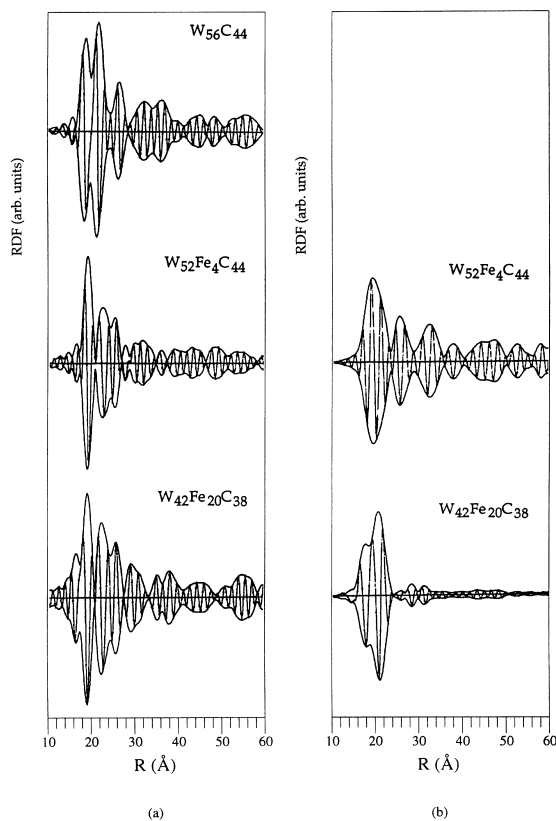


Fig. 6. Fourier transforms of the EXAFS spectra recorded at W-L (a) and Fe-K (b) edges for two W-Fe-C films with different iron contents. For reference, results from a W-C film are also presented.

The Fourier transforms of the EXAFS spectra recorded at the tungsten L and iron K edges for two W-Fe-C films (one crystalline and one amorphous) are presented in Fig. 6. Data for a W-C film are also presented for reference. The  $W_{56}C_{44}$  film shows a typically crystalline tungsten L edge spectrum with some well defined shells of neighbours. The oscillations in low- $r$  side of the first peak are due to determination errors of the Fourier transform and are not structural in origin. The differences between the W-L spectra of films with and without iron concern essentially the second coordination shell, the RDF intensity of which is lower for the films with iron. Both W-Fe-C films have W-L EXAFS spectra typical of ordered materials with well defined RDF peaks. Concerning

Table 2. Structural results of two W-Fe-C films taken from the least square fittings of the W-L EXAFS spectra for the first three shells of neighbours. Results for a W-C film are also presented for comparison

Film	1st Shell	2nd Shell	3rd Shell
	N.n./R(Å)	N.n./R(Å)	N.n./R(Å)
$W_{56}C_{44}$	4.9/2.17	4.9/2.17	4.6/2.13
$W_{52}Fe_4C_{44}$	12.0/2.92	11.2/2.92	10.0/2.97
$W_{42}Fe_{20}C_{38}$	6.5/3.62	6.5/3.62	6.0/3.67

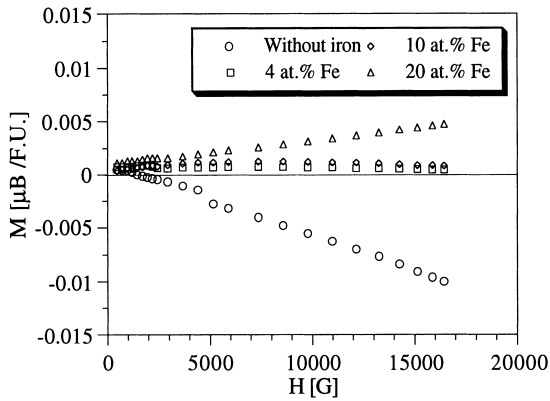


Fig. 7. Room temperature magnetization curves of some W-Fe-C films.

the Fe-K spectra, the Fourier transform of the iron-lean film ( $W_{53}Fe_4C_{44}$ ) differs significantly from the Fourier transform pattern for the film richer in iron ( $W_{42}Fe_{20}C_{38}$ ): the former shows some well defined shells of neighbours with an overlapping of the first two RDF peaks, while the latter is characteristic of disordered structures. The structural results of the least square fittings of the normalized W-L EXAFS spectra [ $\chi(k)$  vs  $k$ ] for the first three shells of neighbours are presented in Table 2.

Figure 7 shows the room temperature magnetization curves of some W-Fe-C films. Once again, data for a W-C film is presented as reference. The magnetization of the  $W_{56}C_{44}$  film varies decreasingly with the increase of the magnetic field. As the

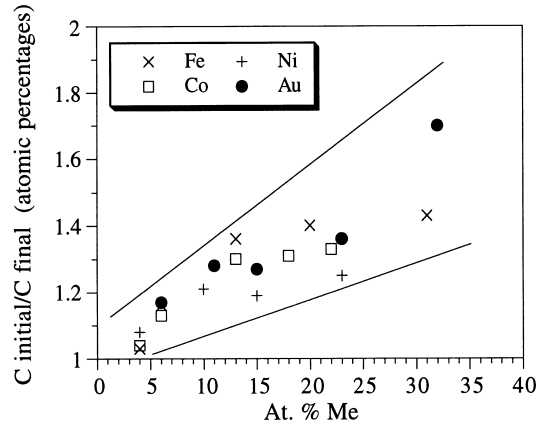


Fig. 8. Ratio between the initial and final carbon contents of various W-Me-C systems as a function of the Me content in the films.

iron content rises, the magnetization signal becomes positive and of greater magnitude.

### 3.2. Thermal behaviour

Figure 8 shows the relation between the carbon composition of the W-Me-C films on steel substrates in the as-deposited state and after 1 h annealing at 750°C. In contrast to the W-Me-C films with Me = Fe, Co, Ni or Au, films with titanium or chromium do not lose carbon during the successive annealings.

Figure 9 shows two examples of the SIMS composition-depth profiles obtained for heat treated W-Me-C films on steel substrates. The SIMS pro-

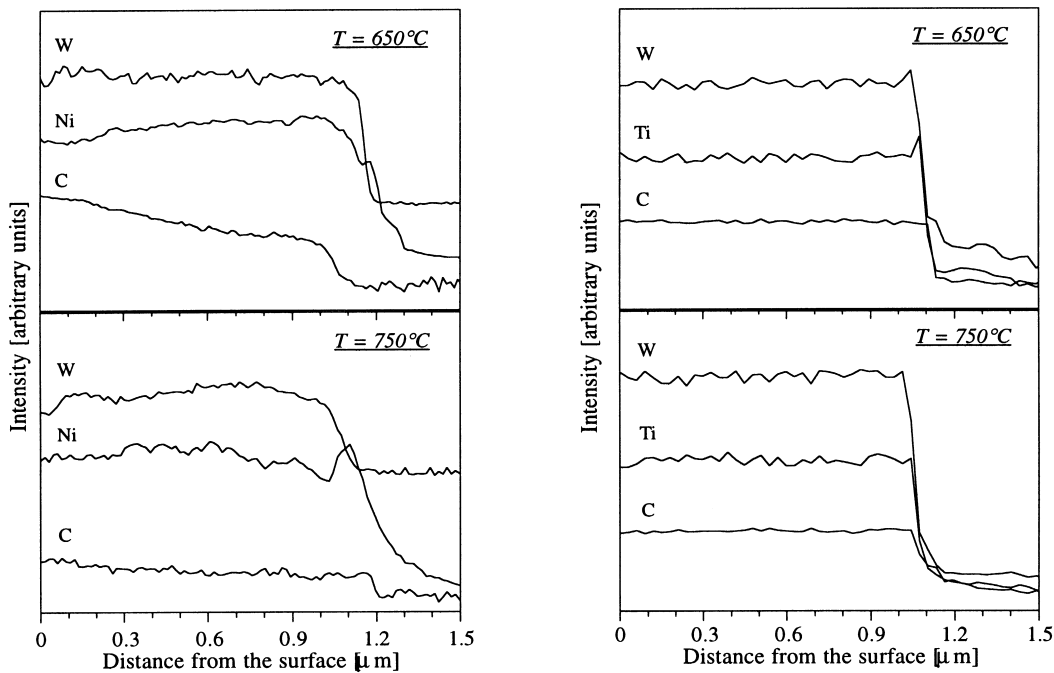


Fig. 9. Typical SIMS sputter depth profiles representative for the two behaviours of the heat-treated (a)  $W_{56}Ti_8C_{36}$  and (b)  $W_{50}Ni_{10}C_{40}$  films on high-speed steel substrates.

Table 3. XRD structural results for the W–C and W–Me–C (Me = Ti, Cr, Fe, Co, Ni, Au) films annealed at 650, 700 and 750°C

Composition	Annealing temperature		
	$T = 650^\circ\text{C}$	$T = 700^\circ\text{C}$	$T = 750^\circ\text{C}$
$\text{W}_{56}\text{C}_{44}$	$\beta\text{-WC}_{1-x} + \text{WC}$	$\beta\text{-WC}_{1-x} + \text{WC} + \text{W}_2\text{C}$	$\beta\text{-WC}_{1-x} + \text{WC} + \text{W}_2\text{C}$
W–Ti–C and W–Cr–C	$\beta\text{-MC}_{1-x}$	$\beta\text{-MC}_{1-x}$	$\beta\text{-MC}_{1-x}$
$\text{W}_{52}\text{Fe}_4\text{C}_{44}$	$\beta\text{-MC}_{1-x} + \text{MC}$	$\beta\text{-MC}_{1-x} + \text{MC}$	$\beta\text{-MC}_{1-x} + \text{MC} + \text{M}_2\text{C}$
$\text{W}_{52}\text{Fe}_6\text{C}_{42}$	$\beta\text{-MC}_{1-x} + \text{MC}$	$\beta\text{-MC}_{1-x} + \text{MC}$	$\beta\text{-MC}_{1-x} + \text{MC} + \text{M}_2\text{C}$
$\text{W}_{46}\text{Fe}_{13}\text{C}_{41}$	A + $\text{M}_2\text{C}$	A + $\text{M}_2\text{C}$	$\text{M}_2\text{C}$
$\text{W}_{42}\text{Fe}_{20}\text{C}_{38}$	A + $\text{M}_2\text{C}$	A? + $\text{M}_2\text{C} + \text{M}_6\text{C}$	$\text{M}_2\text{C} + \text{M}_6\text{C}$
$\text{W}_{36}\text{Fe}_{31}\text{C}_{33}$	A + $\text{M}_6\text{C}$	$\text{M}_6\text{C}$	$\text{M}_6\text{C}$
$\text{W}_{53}\text{Co}_4\text{C}_{43}$	$\beta\text{-MC}_{1-x} + \text{MC}$	$\beta\text{-MC}_{1-x} + \text{MC}$	$\beta\text{-MC}_{1-x} + \text{MC} + \text{M}_2\text{C}$
$\text{W}_{52}\text{Co}_6\text{C}_{42}$	$\beta\text{-MC}_{1-x} + \text{MC}^\dagger$	$\beta\text{-MC}_{1-x} + \text{MC}$	$\beta\text{-MC}_{1-x} + \text{MC} + \text{M}_2\text{C}$
$\text{W}_{48}\text{Co}_{13}\text{C}_{39}$	A + $\text{M}_2\text{C}$	A + $\text{M}_2\text{C}$	$\text{M}_2\text{C}$
$\text{W}_{44}\text{Co}_{18}\text{C}_{38}$	A + $\text{M}_2\text{C}$	A + $\text{M}_2\text{C} + \text{M}_6\text{C}$	$\text{M}_2\text{C} + \text{M}_6\text{C}$
$\text{W}_{45}\text{Co}_{22}\text{C}_{37}$	A + $\text{M}_2\text{C}$	A + $\text{M}_2\text{C} + \text{M}_6\text{C}$	$\text{M}_2\text{C} + \text{M}_6\text{C}$
$\text{W}_{56}\text{Ni}_4\text{C}_{40}$	$\beta\text{-MC}_{1-x}$	$\beta\text{-MC}_{1-x} + \text{MC} + \text{M}_2\text{C}$	$\text{MC} + \text{M}_2\text{C}$
$\text{W}_{53}\text{Ni}_6\text{C}_{41}$	A + MC	MC + $\text{M}_2\text{C}$	$\text{M}_2\text{C} + \text{MC} + \text{M}_6\text{C}^\dagger$
$\text{W}_{51}\text{Ni}_{10}\text{C}_{39}$	A + $\beta\text{-M}_{1-x} + \text{MC}$	MC + $\text{M}_6\text{C} + (\text{Ni})$	MC + $\text{M}_6\text{C} + (\text{Ni})$
$\text{W}_{47}\text{Ni}_{15}\text{C}_{38}$	A + (Ni) + $\text{MC}^\dagger$	A + (Ni) + MC	(Ni) + $\text{MC} + \text{M}_6\text{C}$
$\text{W}_{39}\text{Ni}_{23}\text{C}_{38}$	(Ni) + MC	(Ni) + MC	(Ni) + MC
$\text{W}_{52}\text{Au}_6\text{C}_{42}$	$\beta\text{-MC}_{1-x}$	$\beta\text{-MC}_{1-x} + \text{M}_2\text{C}$	$\text{M}_2\text{C}$
$\text{W}_{49}\text{Au}_{11}\text{C}_{40}$	$\beta\text{-MC}_{1-x} + \text{M}_2\text{C}$	$\text{M}_2\text{C} + \text{M}_6\text{C}$	$\text{M}_2\text{C} + \text{M}_6\text{C}$
$\text{W}_{47}\text{Au}_{15}\text{C}_{38}$	$\beta\text{-MC}_{1-x}$	$\text{M}_2\text{C} + \text{M}_6\text{C}$	$\text{M}_2\text{C} + \text{M}_6\text{C}$
$\text{W}_{37}\text{Au}_{23}\text{C}_{34}$	$\text{M}_2\text{C} + \text{M}_6\text{C}$	$\text{M}_6\text{C} + (\text{Au})$	$\text{M}_6\text{C} + (\text{Au})$
$\text{W}_{38}\text{Au}_{32}\text{C}_{30}$	$\text{M}_2\text{C} + \text{M}_6\text{C} + (\text{Au})$	$\text{M}_2\text{C} + \text{M}_6\text{C} + (\text{Au})$	$\text{M}_6\text{C} + (\text{Au})$

A = Amorphous.

$^\dagger$ Signs of the phase were detected in the XRD diffractograms

files recorded from films with Me = Fe, Co, Ni or Au [Fig. 9(a)] revealed that carbon had diffused from the films into the steel. The shapes of the profiles obtained from films with Me = Ti or Cr annealed at 650, 700 and 750°C [Fig. 9(b)] are similar, although showing no evidence of diffusion from the films into the substrates or vice-versa.

The structural characterization of the W–Me–C films deposited on steel substrates was studied by XRD after each furnace annealing. The results are presented in Table 3. As can be seen, all films except W–Ti–C and W–Cr–C change structurally with temperature. The resultant structures depend on the type and content of the element Me in the films. The structural behaviour of films without element Me is characterized by the formation of WC +  $\text{W}_2\text{C}$  from  $\beta\text{-WC}_{1-x}$ . The addition of titanium or chromium to the W–C system stabilizes the crystalline as-deposited structure ( $\beta\text{-MC}_{1-x}$ ) during annealing. In fact, no structural transformations of both W–Ti–C and W–Cr–C systems were observed during successive *anneals* up to 750°C. Iron and cobalt play similar roles in the structural evolution of the (W–C)-based films. During annealing the sequence of structural transformations with increasing Me and temperature is as follows:  $\beta\text{-MC}_{1-x}$  or amorphous  $\rightarrow \text{MC} \rightarrow \text{M}_2\text{C} \rightarrow \text{M}_6\text{C}$ . Besides these carbides, the addition of nickel or gold to the W–C system leads to the formation of Ni-rich or Au-rich terminal solid solutions during annealing. The higher the content of both nickel and gold elements in the films, the lower the temperature at which these solid solutions appear.

In order to determine the influence of the Me transition metals on the stability of the as-deposited systems, W–Me–C films with Me = Ti, Cr, Fe, Co

and Ni were detached from the substrates and studied *in situ* by TEM/ED and ATD during continuous heating up to  $\approx 1000^\circ\text{C}$ . X-ray diffraction was used as a complementary technique for phase identification after cooling of the samples. Table 4 shows a compilation of the results obtained by TEM/ED and ATD. Each peak detected in the ATD curves is associated with the structural transformation observed and characterized by TEM/ED. The final structure of the W–Me–C films determined by XRD after cooling from 1000°C is presented in the same table.

## 4. DISCUSSION

### 4.1. As-deposited state

The chemical analysis of the W–Me–C films confirms that sputtering of multicomponent targets leads to films enriched in elements with higher atomic weight and lean in lighter elements [9, 10]. The  $\text{W}_{56}\text{C}_{44}$  film is a typical example of this. When the WC stoichiometric target is bombarded with  $\text{Ar}^+$  ions, there is a preferential emission of carbon and the target surface becomes enriched in tungsten, approaching a  $\text{WC}_{1-x}$  composition. From this moment, the preferential sputtering of carbon is counterbalanced by the deficit of this element in the surface, and therefore the same number of carbon and tungsten species are sputtered from the target. Thus, the carbon impoverishment of the W–C films must occur essentially during its formation by the bombardment of the reflected neutral species and not by eventual diffusion into the steel substrates, SIMS results support this idea: the  $\text{C}^-$  and  $\text{W}^+$  sputter depth profiles measured in both film and substrate are horizontal and the film/substrate

Table 4. Compilation of the structural results obtained from the W–Me–C films (Me = Ti, Cr, Fe, Co, Ni) during continuous heating up to 1000°C

Composition	Structural transformations with temperature	Final structure
W <sub>56</sub> C <sub>44</sub>	██████████ $\beta\text{-WC}_{1-x} \xrightarrow{845^\circ\text{C}} \text{W}_2\text{C} + \text{WC}$	W <sub>2</sub> C + WC
W–Ti–C and W–Cr–C	██████████ $\beta\text{-MC}_{1-x} \xrightarrow{\approx 960^\circ\text{C}} \text{M}_2\text{C} + \text{MC}^\ddagger$	M <sub>2</sub> C + MC <sup>†</sup>
W <sub>52</sub> Fe <sub>4</sub> C <sub>44</sub>	██████████ $\beta\text{-MC}_{1-x} \xrightarrow{856^\circ\text{C}} \text{M}_2\text{C} + \text{MC}$	M <sub>2</sub> C + MC
W <sub>46</sub> Fe <sub>13</sub> C <sub>41</sub>	██████████ $\text{A} \xrightarrow{758^\circ\text{C}} \text{M}_2\text{C} \quad \text{M}_2\text{C} \xrightarrow{845^\circ\text{C}} \text{MC} + \text{M}_6\text{C}$	M <sub>2</sub> C + MC + M <sub>6</sub> C
W <sub>42</sub> Fe <sub>20</sub> C <sub>38</sub>	██████████ $\text{A} \xrightarrow{700^\circ\text{C}} \text{M}_2\text{C} \quad \text{M}_2\text{C} \xrightarrow{763^\circ\text{C}} \text{MC} + \text{M}_6\text{C}$	M <sub>2</sub> C + MC + M <sub>6</sub> C
W <sub>36</sub> Fe <sub>31</sub> C <sub>33</sub>	██████████ $\text{A} \xrightarrow{695^\circ\text{C}} \text{M}_2\text{C} \quad \text{M}_2\text{C} \xrightarrow{750^\circ\text{C}} \text{MC} + \text{M}_6\text{C}$	MC + M <sub>6</sub> C
W <sub>53</sub> Co <sub>4</sub> C <sub>43</sub>	██████████ $\beta\text{-MC}_{1-x} \xrightarrow{856^\circ\text{C}} \text{M}_2\text{C} + \text{MC}$	M <sub>2</sub> C + MC
W <sub>48</sub> Co <sub>13</sub> C <sub>39</sub>	██████████ $\text{A} \xrightarrow{750^\circ\text{C}} \text{M}_2\text{C} \quad \text{M}_2\text{C} \xrightarrow{850^\circ\text{C}} \text{MC} + \text{M}_6\text{C}$	M <sub>2</sub> C + MC + M <sub>6</sub> C
W <sub>44</sub> Co <sub>18</sub> C <sub>38</sub>	██████████ $\text{A} \xrightarrow{703^\circ\text{C}} \text{M}_2\text{C} \quad \text{M}_2\text{C} \xrightarrow{813^\circ\text{C}} \text{MC} + \text{M}_6\text{C}$	MC + M <sub>6</sub> C
W <sub>45</sub> Co <sub>22</sub> C <sub>37</sub>	██████████ $\text{A} \xrightarrow{706^\circ\text{C}} \text{M}_2\text{C} \quad \text{M}_2\text{C} \xrightarrow{760^\circ\text{C}} \text{MC} + \text{M}_6\text{C}$	MC + M <sub>6</sub> C
W <sub>56</sub> Ni <sub>4</sub> C <sub>40</sub>	██████████ $\beta\text{-MC}_{1-x} \xrightarrow{862^\circ\text{C}} \text{M}_2\text{C} + \text{MC}$	M <sub>2</sub> C + MC
W <sub>51</sub> Ni <sub>10</sub> C <sub>39</sub>	██████████ $\text{A} \xrightarrow{735^\circ\text{C}} \text{MC} + (\text{Ni})$	MC + (Ni)
W <sub>47</sub> Ni <sub>15</sub> C <sub>38</sub>	██████████ $\text{A} \xrightarrow{705^\circ\text{C}} \text{MC} + (\text{Ni})$	MC + (Ni) + M <sub>6</sub> C
W <sub>39</sub> Ni <sub>23</sub> C <sub>38</sub>	██████████ $\text{A} \xrightarrow{680^\circ\text{C}} \text{MC} + (\text{Ni})$	MC + (Ni) + M <sub>6</sub> C

<sup>†</sup>This structural transformation was only observed for W–Ti–C and W–Cr–C films with low titanium and chromium contents (< 10at.%). Films richer in one of these metals are stable up to the maximal temperature achieved in this work.

██████████ Stability of the structure of the as-deposited films.

interfaces are well defined, which is incompatible with any diffusion of either carbon or tungsten.

Concerning the synthesis of the W–Me–C systems, the carbon deficit in the films is related to the concentration of element Me. For all but the W–Au–C systems the value of the W/C ratio decreases with the Me content increasing. This confirms previous studies which showed a direct dependence of the atomic weight of the nearest neighbours of carbon on its sputtering yield in multicomponent materials [6, 7]. On the basis of the present work, one might conclude that the addition of a metal with an atomic weight lighter than tungsten decreases the W/C ratio, while the inverse situation occurs for heavier metals. This is the case for the additions used in this work: Cr, Fe, Co, Ni and Pd are lighter than tungsten, decreasing the W/C ratio of the films produced from stoichiometric WC targets by sputtering. In contrast, the higher the gold content, the higher the carbon deficit of the W–Au–C films due to the higher atomic weight of gold compared to tungsten.

The preferential emission of carbon during formation of the W–C and W–Me–C films allows the formation of metastable phases instead of the equilibrium MC phase expected from the W–C phase diagram [11]. According to this diagram,  $\beta\text{-MC}_{1-x}$  has a NaCl-type structure existing only above 2530°C. The occurrence of this metastable structure in sputtered (W–C)-based films seems to be due to its wide range of composition and strong cohesion of the metal–carbon covalent bonds [12]. According to Cottrell [12], the strong cohesion of the NaCl-type carbides of groups IVA–VIA is essentially due to strong covalent bonds between the *p* electrons of the non-metal atom and the *d* electrons of the tran-

sition metal (one in the *s* band, two in *pd $\sigma$*  bonding orbitals, and one in the *pd $\pi$*  bonding orbitals). In the case of the binary stoichiometric WC f.c.c. carbide, not all the six valency electrons of tungsten ([Xe] 4<sup>f</sup>145<sup>d</sup>4<sup>6s</sup>2) are used in the W–C bonds. In other words, in WC there is a certain degree of W–W bonding, its contribution towards the cohesion of the carbide being minor as compared to W–C bonding. For non-stoichiometric WC<sub>1-x</sub> there is more W–W bonding amongst the nearest neighbours and the density of states is reduced in proportion to the smaller fraction of carbon atoms. In addition, the existence of vacant carbon sites gives rise to weak bonds, with second nearest W–W neighbours across the vacancies. Replacement of tungsten by other transition metals occurs with a decrease of metal-to-carbon composition ratio in the carbide. Thus, depending on the affinity of carbon for the addition metal, MC<sub>1-x</sub> carbides with different stabilities may be formed. In fact, as it will be seen later, the thermal stability of the W–Me–C films depends on the element Me and is higher for strong carbide-forming elements.

Concerning the amorphous (W–C)-based systems, the results show that their atomic arrangement is not completely random, but maintains a degree of short range order (less than 20 Å). EXAFS experiments indicate that these films can be regarded as an atomically heterogenous mixture formed by regions of very small crystallites of MC<sub>1-x</sub> rich in tungsten and regions of “real” amorphous phase rich in element Me.

The amorphization of the (W–C)-based films has been discussed in terms of the following effects: (i) distortion of the  $\beta\text{-MC}_{1-x}$  (*M* = W, Me) lattice due to the difference between the atomic radii of the

two metals, and (ii) lower carbon affinity for the later transition metal than for tungsten [5–7]. The results now obtained show that the amorphization of the W–Me–C may not be attributed only to these two effects. In fact, despite the differences of the atomic sizes between tungsten and the elements palladium and gold being almost identical, palladium induces amorphous films, whilst gold does not. Furthermore, both elements are non-carbide-forming metals. Thus, from these facts, it is obvious that one has to consider other factors in predicting the occurrence of the amorphous phases. One of these factors is related with the number and strength of the metal–carbon covalent bonds. According to the model of Cottrell [12], replacement of tungsten by a later transition metal (more *d* electrons) enables more *ddσ* bonding orbitals to fill (metal–metal nearest neighbours). This induces weakening of the metal–carbon covalent bonds and strengthening of the metal–metal bonds, its contribution to the cohesion of the carbide being of little importance. Conversely, the addition of a strong carbide-forming element gives rise to a larger number of strong metal–carbon bonds and promotes crystallisation. This was recently confirmed in a study on the influence of titanium on amorphous W–Co–C films [13]. The results showed that, in fact, it is possible to obtain crystallinity in these films by the addition of small amounts of titanium. This metal tends to enhance ordering of the structure giving rise to spontaneous crystallization of  $\beta$ - $MC_{1-x}$  during formation of the films.

#### 4.2. Thermal behaviour

The thermal behaviour of the (W–C)-based films is strongly dependent on their composition and structure. Concerning the crystalline as-deposited films, the decomposition of the  $MC_{1-x}$  phase is shown to take place in two different ways, depending on the composition. In fact, all but the gold-rich films decompose during annealing into  $MC + M_2C$ . XRD scans performed on films annealed 1 h at 650°C show that the  $MC$  phase is the first product of the  $MC_{1-x}$  decomposition. The  $M_2C$  phase appears later, as the result of a carbon impoverishment of the remaining  $MC_{1-x}$  phase. The thermal stability of this phase is affected by its chemical composition. The addition of a transition metal to the W–C system increases the temperature of the  $MC_{1-x} \rightarrow MC + M_2C$  reaction, in particular if this metal is either titanium or chromium. This might be the result of the higher carbon deficit of the W–Me–C films compared to the W–C binary ones. Moreover, as has been seen, the incorporation of strong carbide-formers (Ti and Cr) to W–C increases the number of strong metal–carbide bonds and, consequently, the stability of the films. Both WC and  $W_2C$  phases have been reported in (W–C)-based films deposited by different techniques such as plasma spraying [14,15], chemical vapour

deposition [16,17] and r.f. sputtering [2,4,18–20]. They may be formed either during the growth of the films (as-deposited structure) or during annealing [4,6–8]. According to the W–C phase diagram [11], for temperatures lower than 1300°C the  $W_{56}C_{44}$  film lies in a two-phase region of W + WC. The  $W_2C$  phase is not predicted for these temperatures. This confirms that the decomposition of a metastable phase (such as  $MC_{1-x}$ ) could lead to the formation of other metastable intermediate phases, e.g.  $M_2C$ , before the equilibrium ones predicted from the phase diagrams [21,22]. Concerning the gold-rich W–Au–C films, the decomposition of the  $MC_{1-x}$  phase leads to the formation of  $M_2C$ ,  $M_6C$  and an Au-rich solid solution (Au). It should be pointed out that since gold does not form carbides [23], both  $M_2C$ , and  $M_6C$  phases must be formed essentially by tungsten, which allows the appearance of a terminal Au-rich solid solution. The higher the initial carbon deficit in the films, the lower is the temperature of this solid solution occurrence. Since  $WC_{1-x}$  and (Au) are partially intersoluble (they are both of cubic structure) the formation of (Au) may occur from structural domains of  $MC_{1-x}$  rich in gold. Rejection of tungsten from  $MC_{1-x}$  allows the formation of tungsten-rich phases such as  $M_2C$  and  $M_6C$ . Based on the SIMS results, it is likely that these carbides may contain a certain percentage of iron. In fact, it was observed that annealing of these films sputtered on steel substrates leads to the migration of some iron atoms from the steel into the films, in particular for films lean in carbon, i.e. rich in gold.

Regarding the crystallization study of the as-deposited amorphous systems, the structure evolution of the W–Ni–C films differs from that of the W–(Fe,Co)–C films with similar concentration of the alloying addition: whereas the crystallisation mechanism of the amorphous as-deposited W–Ni–C films is essentially characterized by the formation of  $\alpha$ -Ni +  $MC$ , W–(Fe,Co)–C films decompose upon crystallisation into  $M_2C + M_6C + MC$ . The different crystallisation characteristics have been explained by the higher solubility of tungsten in nickel compared with that of tungsten in iron or cobalt [24]. Therefore, in the case of W–Ni–C films, the  $\alpha$ -Ni solid solution could contain a certain concentration of tungsten, thereby preventing the formation of tungsten-rich carbides, e.g.  $M_2C$  or  $M_6C$ . Moreover, it is known that the stability of these carbides is higher for iron or cobalt than for nickel [23], favouring their appearance in the W–(Fe,Co)–C films.

In the light of the present results it is possible to discuss the application of sputtered (W–C)-based films for industrial materials, e.g. cutting tools or wear-resistant mechanical components. Concerning the traditional W–Co–C system, one may conclude that the crystalline films allow for higher service temperatures than the amorphous ones, without

structural transformations. However, the application of these films in such technological fields requires the incorporation of an element capable to stabilize the as-deposited structure and to slow down the migration of carbon atoms into the substrate. Titanium or chromium seem to be adequate elements for this purpose. Another approach is to deposit the films on substrates richer in carbon, e.g. sintered WC. This might contribute to the increase of the thermal stability of the films, impeding the migration of carbon into the substrates.

The main problem in optimizing hard coatings is to increase the toughness while maintaining a high hardness. Concerning the structural evolution of both W–Co–C and W–Fe–C films, none of the structural changes observed during their heat treatment lead to the occurrence of a fine-grained soft terminal solid solution capable of controlling crack propagation by strain energy dissipation. This problem might be overcome by the incorporation of small amounts of nickel ( $\approx 10$  at.%) to (W–C)-based coatings. In fact, these amorphous as-deposited films may act as precursors for multiphase fine-grained microstructures of (Ni) + MC by means of subsequent heat treatments. Given the fact that the studied W–Ni–C films have a similar chemical composition as ceramic W–Ni–C bulk materials, but with a finer-grained structure, the annealed W–Ni–C films could in the future be used as coatings for mechanical applications.

## 5. CONCLUSIONS

The results show that the structure of the as-deposited (W–C)-based films is characterised by different degrees of structural order depending on their chemical composition. Among the transition metals studied, most of them form a f.c.c. phase of  $\beta$ - $MC_{1-x}$  with tungsten and carbon with  $1-x$  extending from about 1 to 0.6; however, the films become amorphous with the addition of small amounts of VIIIA transition metal, e.g. iron, cobalt, nickel or palladium. The atomic arrangement of these films is not completely random but maintains a degree of short range order (less than 20 Å); their structure is formed by small  $\beta$ - $MC_{1-x}$  crystallites with the size of a few unity cells, surrounded by a disordered phase rich in element Me.

The structural behaviour of the W–Me–C films subjected to high temperatures depends on their chemical composition, particularly on the carbon affinity for the transition metal Me. The films with strong or moderate carbide-forming elements (Ti or

Cr) do not show any change, neither in their chemical nor structural composition, in the range of temperatures studied. However, the films formed by W, C and a weak or non-carbide-forming metal (Fe, Co, Ni, Pd or Au), besides showing different structural transformations, tend to lose carbon to the substrates.

*Acknowledgements*—The authors are grateful for the measurements of the EXAFS spectra by M. Jauouen of Université de Poitiers, France.

## REFERENCES

1. Srivastava, P. K., Vankar, V. D. and Chopra, K. L., *Thin Solid Films*, 1988.
2. Jang, H.-J., Zhao, X.-A. and Nicolet, M. A., *Thin Solid Films*, 1988, **158**, 37.
3. Keller, G., Barzer, I., Erz, R., Dotter, W., Ulrich, S., Jung, K. and Ehrhardt, H., *Fresenius J. Anal. Chem.*, 1991, **341**, 349.
4. Cavaleiro, A., Vieira, M. T. and Lemperière, G., *Thin Solid Films*, 1991, **197**, 237.
5. Trindade, B. and Vieira, M. T., *Thin Solid Films*, 1991, **206**, 318.
6. Trindade, B., Vieira, M. T. and Grosse, E. B., *Mat. Sci. Engng. A*, 1994, **174**, 165.
7. Trindade, B., Vieira, M. T. and Grosse, E. B., *Thin Solid Films*, 1994, **252**, 82.
8. Trindade, B., Vieira, M. T. and Grosse, E. B., *Acta metall. mater.*, 1995, **43**(1), 93.
9. Sigmund, P., *J. Vac. Sci. Technol.*, 1977, **214**, 152.
10. Winters, H. F., *J. Vac. Sci. Technol.*, 1982, **3**, 493.
11. Rudy, E., in *Compendium of Phase Diagram Data: Ternary Phase Equilibria in Transition Metal–Boron–Silicon Systems*, part 5. US Air Force AFML-TR-65, May 1969.
12. Cotrell, H. A., *Mater. Sci. and Technol.*, 1994, **10**, 22.
13. Trindade, B., Vieira, M. T. and Bauer-Grosse, E., *Surface Coatings and Technology*, 1995, **74**(75), 802.
14. Tu, S., Chao, S. and Lin, C., *J. Vac. Sci. Technol. A*, 1985, **3**, 2479.
15. Vinayo, M. E., Kassabji, F., Guyonnet, J. and Fauchais, P., *J. Vac. Sci. Technol. A*, 1985, **3**, 2483.
16. Archer, N. J. and Yee, K. K., *Wear*, 1978, **48**, 237.
17. Gard, D., Dyer, P. N., Dimos, D. B., Sunder, S., Hinterman, H. E. and Maillat, M., *Ceram. Eng. Sci. Proc.*, 1988, **9**, 1215.
18. Taylor, K. A., *Thin Solid Films*, 1977, **40**, 189.
19. Eser, E., Ogilvie, R. E. and Taylor, K. A., *J. Vac. Sci. Technol. A*, 1978, **15**, 396.
20. Eser, E., Ogilvie, R. E. and Taylor, K. A., *Thin Solid Films*, 1980, **67**, 265.
21. Hwang, C. H., Kang, S. and Cho, K., *Scripta metall.*, 1985, **19**, 1403.
22. Kim, J. J., Moine, P. and Stevenson, D. A., *Scripta metall.*, 1986, **20**, 243.
23. Goldschmidt, H. J., *J. Iron and Steel Institute*, 1948, **December**, 345.
24. Hansen, M., in *Constitution of Binary Alloys*. McGraw-Hill, New York, 1958, p. 519, 735 and 1058.